Int. J. Electrochem. Sci., 16 **(2021)** Article ID: 21088, doi: 10.20964/2021.08.19

International Journal of
ELECTROCHEMICAL
SCIENCE
www.electrochemsci.org

The Effect of Environmental Conditions on Electrochemical Corrosion Behavior of AISI 1018 Low-carbon Steel in Concrete Pore Solution

Ming Li

School of civil engineering, Jilin Jianzhu University, Changchun Jilin 130118, China
E-mail:minglipossess@sina.com

Received: 31 March 2021/ *Accepted:* 17 May 2021 / *Published:* 30 June 2021

The effect of environmental conditions such as dissolved oxygen (DO) and temperature on electrochemical corrosion behavior of AISI 1018 low-carbon steel in concrete pore solution (CPS) were investigated. The corrosion behavior of low-carbon steel was determined using electrochemical impedance spectroscopy (EIS) and potentiodynamic polarization methods at temperatures ranging from 20 to 40 ºC and DOES concentration from 0.5 ppm to 4.5 ppm. The corrosion rate of steels increased with increasing ambient temperatures. The electrochemical corrosion resistance was observed to be higher in CPS with lower DO concentrations. The SEM analysis shows that the metal dissolution rate was more intense in CPS with higher DO levels.

Keywords: Dissolved oxygen; Electrochemical corrosion behavior; AISI 1018 low-carbon steel; Cement pore solution

1. INTRODUCTION

Corrosion resistance of reinforced concrete can be an important factor in its durability [1, 2]. Low-corrosion resistance may predictably cause significant and expensive repair work in the concrete [3, 4]. It is clear that the primarily protective environment that concrete structures provide for steel rebar is due to its alkaline nature [5, 6]. It usually happens in positive or passive corrosion potential for steel embedded in concrete [4, 7]. When corrosive ions for example chlorides penetrate into the concrete structure, the environment may become promising for corrosion of steel [8]. When corrosive ions reach dangerous amounts, the potential becomes more active, and hence a shift in values of corrosion potential is often related to the intrusion of corrosive ions [9]. It may result in an increase in the rate of corrosion. Consistent with classical corrosion theory [1, 10, 11], species existent in the environment can influence the anodic reaction, the cathodic reaction, or both through either preventing the reaction. Baek et al. [12] determined which dissolved oxygen (DO) into a NaCl medium plays an

important role for the creation of anodic oxide layer, as well as the kinetics of film growth on low carbon steels. Eyu et al. [13] reveals that an inferior DO content in coal-seam gas produced water increased with decreasing corrosion potential. With respect to the decrease of O_2 on carbon steels, Tachibana et al. [14] shows that the corrosion potential is primarily determined by cathodic polarization into oxygenated environments. In fact, the decrease of H_2O accompanied by H_2 production also shows a significant role in steel corrosion, particularly for the alkaline solution in low DO [15].These works considered the effect of DO on the corrosion behavior of steel at ambient temperature. However, some studies on the effect of DO on steel corrosion behavior have been conducted at a single temperature. Therefore, the temperature and DO influence on the corrosion resistance of carbon steel rebar in concrete pore solution (CPS) has not been studied systematically.

The aim of this study is to consider the effects of temperature and DO on the electrochemical corrosion behavior of the carbon steel in typical CPS and to experimentally evaluate the electrochemical parameters.

2. MATERIALS AND METHOD

To investigate the effects of temperature and DO on the electrochemical corrosion behavior of steel in cement pore solution, AISI 1018 low-carbon steels with 25cm long and 0.8cm diameter were used. The chemical composition of AISI 1018 steel is 0.17wt% C, 0.75wt% Mn, 0.03wt% P, 0.04wt% S and Fe (Balance). All steels were cleaned by acetone and washed in DI water and then air-dried. The ends of steel specimens are coated by an epoxy-resin.

To prepare concrete pore solution (CPS), a mixture of NaOH (0.2 mol/dm^3), $Ca(OH)_2$ (0.3 mol/dm^3) and KOH (0.5 mol/dm^3) with pH-value 13 was used. The electrochemical tests were performed by a three-electrode system consisting of AISI 1018 steels (working electrode), a graphite rod (counter) and saturated calomel (reference electrode). The specimens were exposed to the CPS including 3wt% NaCl. The exposure temperatures were 20, 25, 30, 35 and 40ºC as a seasonal change in temperature in a hot-CPS environment.

Electrochemical impedance spectroscopy (EIS) assessment was used in the range of frequencies from 1mHz to 10kHz at the open-circuit voltage with ±10mV perturbation. The potentiodynamic polarization experiment was done at a scanning rate of 0.5mV/s. A scanning electron microscope was used to examine the surface morphologies of low-carbon steel specimens.

The experiment solutions were bubbled through different O_2/N_2 gas mixes for 5 hours at ambient pressure and 75ºC. The values of DO concentration for the solutions under various O_2 volume conditions were determined by polarographic technique (JSPS-605 F DO Analyzer) [16].

3. RESULTS AND DISCUSSION

Concentration of DO is reduced by nitrogen purging time (NPT). In this work, the NPT also led to a slight decrease in temperature. For example, at initial purging, the temperature of the test solution

was 20 °C, with 4 ppm DO. When DO concentration significantly decreased to 0.5 ppm after 12h, the temperature reduced to 19.4 °C which can be ignored. The temperature reduction with NPT was because of the nitrogen cooling effect.

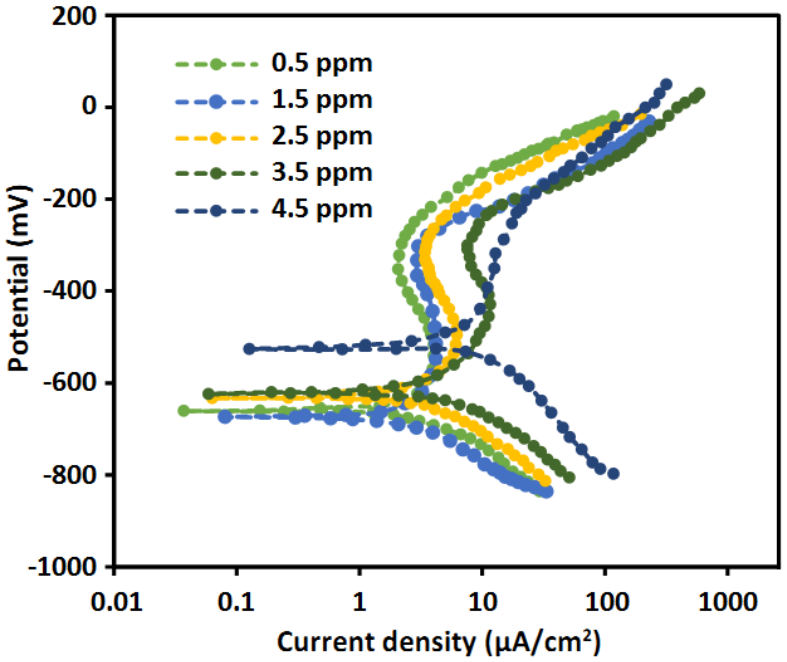

Figure 1. Polarization plots of low-carbon steel in concrete pore solution in different concentrations of dissolved oxygen at 20 °C

Table 1. Polarization parameters of low-carbon steel in cement pore solution in different concentrations of dissolved oxygen

DO concentration (ppm)	Corrosion current density (µA/cm^2)	Corrosion potential (V)	βa (mV/des)	-βc (mV/dec)
0.5	3.4	-0.654	174	311
1.5	4.8	-0.663	154	223
2.5	5.2	-0.617	185	228
3.5	5.7	-0.614	191	232
4.5	17.5	-0.528	213	242

Figure 1 indicates the polarization plots of low-carbon steel in CPS in different concentrations of DO. As shown, the anodic polarization was increased with no retardation at 3 ppm DO content, while one anodic peak was observed in solutions containing 0.5 ppm and 2.5 ppm DO. Furthermore, the current density rises with corrosion potential below -0.6 V_{SCE}, showing iron dissolution while at corrosion potentials higher than -0.6 V_{SCE}, the current density falls, revealing formation of passivation layers. The cause of this behavior could be the result of corrosion products. Such as, $Fe(OH)_2$ shaped on the steel surface, consistent with the following reaction [17]:

$$Fe + 2H_2O \rightarrow Fe(OH)_2 + 2H^+ + 2e^- \quad (1)$$

$Fe(OH)_2$ creates a defective hydrous layer between the solution and steel sample, and thus delays the anodic current densities [18]. As revealed in Table 1, the corrosion current densities are reduced by reducing DO concentrations from 17.5 µAcm^2 to 3.4 µAcm^2 at 4.5 ppm to 0.5 ppm, respectively. This shows that a more stable and compact oxide layer was formed at -0.6 V_{SCE} at lower DO. The rise in anodic polarization current by falling DO content at a more positive potential can be related to solubility of corrosion products and negligible oxidation at the surface of steel to create oxide layer by the Kuch mechanism [19].

Figure 2 exhibits the Nyquist and Bode curves for different concentrations of DO in the CPS environment. As shown in figure 1a, the diameter of the semicircle rises with reducing DO content, which shows that reducing DO helps to form a more stable oxide film on the surface of low-carbon steel. A similar trend may be observed in the Bode plots (Fig. 2b), where the impedance rises with falling DO concentrations at low-frequencies. The phase angle indicates a greater peak as DO content reduces. A higher value of phase angle at low-frequency reveals a higher resistance of the steel surface.

The EIS data was fitted by an equivalent circuit model as indicated in Figure 3. R_s presents the solution resistance, R_f and C_f show resistance and capacitance of oxide film, respectively. They are used to simulate high-frequency loops. Furthermore, R_{ct} and C_{dl} indicate the charge-transfer resistance and double layer capacitance, respectively [20].

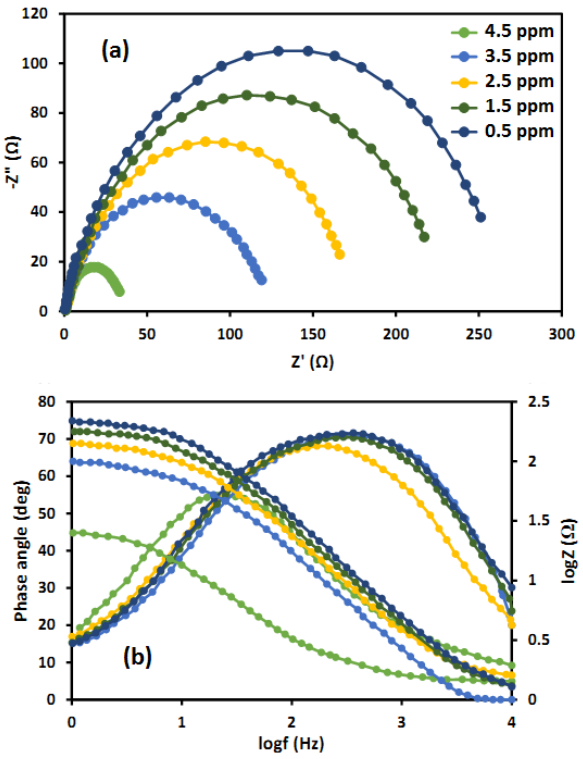

Figure 2. (a) Nyquist and (b) Bode curves of low-carbon steel for different concentrations of dissolved oxygen in concrete pore solution at 20 ºC

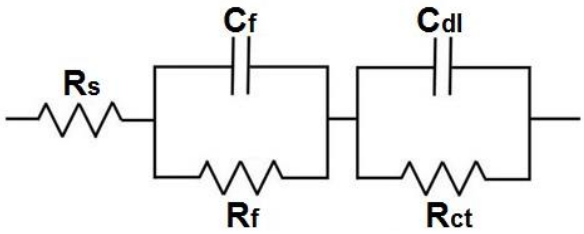

Figure 3. An equivalent circuit

Obtained data exhibited in Table 2 shows that by reducing DO content into the CPS, R_c and R_{ct} increase and C_{dl} and C_f reduce, which can be associated with the passive layer stability on low-carbon steel, improving the corrosion resistance. As shown in table 2, the film resistance (R_f) increases considerably with reducing DO content, indicating the corrosion product on the surface of low-carbon steel was more protective and dense at a relatively low concentration of DO as indicated in Figure 4.

Table 2. Achieved EIS parameters from Nyquist diagrams fitted by a circuit model

DO concentration (ppm)	R_s(Ω)	R_f(Ω)	C_f(mFcm^{-2})	R_{ct}(Ω)	C_{dl}(mFcm^{-2})
0.5	9.8	210	3.1	263	3.9
1.5	10.5	184	3.8	231	4.7
2.5	10.8	136	4.6	172	5.3
3.5	11.2	89	6.2	119	7.2
4.5	12.4	28	14.9	37	19.7

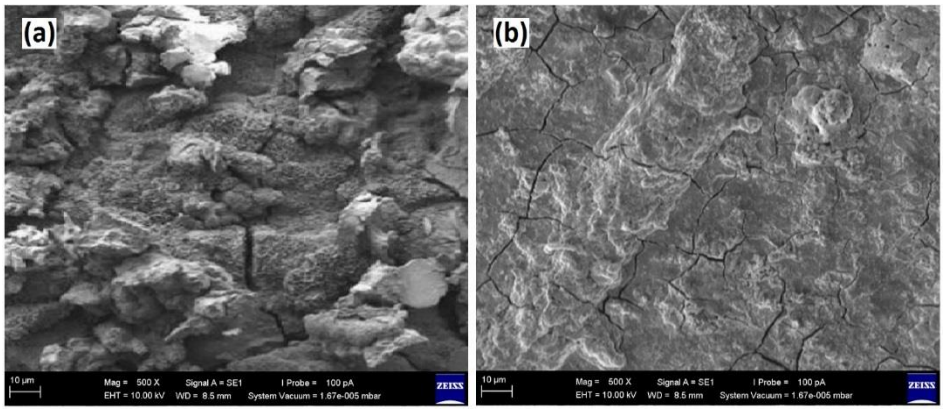

Figure 4. SEM images of low-carbon steel in concrete pore solution (a) 4.5 ppm and (b) 0.5 ppm dissolved oxygen concentrations after 24 hours immersion time at 20 ºC

Figure 5 demonstrates the polarization plots of low-carbon steel exposed to CPS at various ambient temperatures. As shown in Fig. 5, the polarization plots for the steels immersed in CPS at 40ºC temperature shifted to anodic direction, indicating an improvement of the corrosion rate in comparison with other specimens exposed to CPS with lower temperatures. It may be associated with

the reaction rate of Cl ions with Fe which may be considerably affected by the kinetic of reaction by rising temperature, as stated in Eqs. (2) and (3).

$Fe^{2+} + 3Cl^- \rightarrow FeCl_3 + 3e^-$ (2)

$FeCl_3 + 3OH^- \rightarrow Fe(OH)_3 + 3Cl^-$ (3)

Corrosion products with the creation of Fe_2O_3 and $Fe(OH)_2$ as the intermediary product were formed, as shown in Equs (4) and (5).

$Fe^{2+} + 2OH^- \rightarrow Fe(OH)_2$ (4)

$4Fe(OH)_2 + O_2 \rightarrow Fe_2O_3H_2O + 2H_2O$ (5)

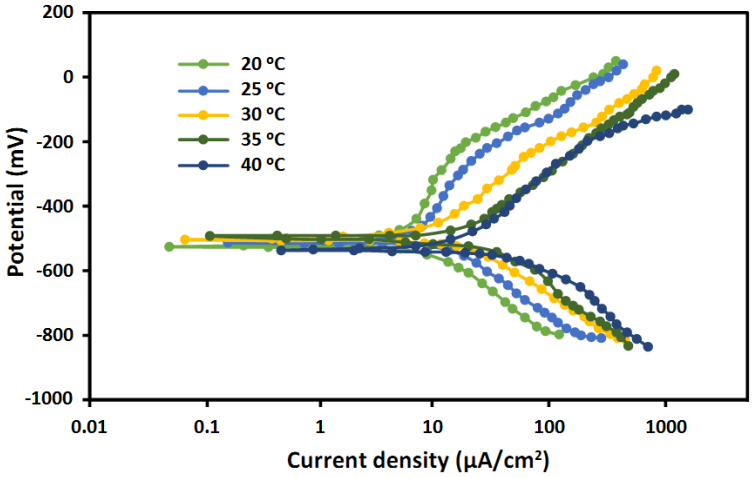

Figure 5. Polarization curves of low-carbon steel exposed to concrete pore solution at various ambient temperatures at 4.5 ppm of dissolved oxygen

Table 3. Polarization parameters of low-carbon steel in concrete pore solution in different temperature at 4.5 ppm of dissolved oxygen

Temperature (°C)	Corrosion current density (µA/cm²)	Corrosion potential (V)	βa (mV/des)	-βc (mV/dec)	CR (mpy)
20	17.5	-0.528	213	242	4.38
25	23.7	-0.524	230	261	7.46
30	28.1	-0.518	245	276	10.25
35	33.9	-0.512	268	297	14.18
40	48.4	-0.531	298	329	18.63

The investigation of Tafel plots permits the consideration of electrochemical corrosion parameters. For example, the corrosion potential (E_{corr}) and corrosion current density (i_{corr}) are summarized in Table 3. The values of cathodic Tafel slope (β_c) were observed in the range 242–329 mV/decade, indicating activation control corrosion. The analysis of the Tafel plot enabled the calculation of i_{corr}, which was then used to calculate the corrosion rate (CR) [21]:

$CR\ (mpy) = [(1.95\times10^5) i_{corr} W]/(\rho A)$ (6)

where A is the contact area between the solution working and electrode (cm^2), ρ is metal density (g/cm^3) and W is equivalent mass of metal (g).

As shown in table 3, when the ambient temperature was increased from 20 to 40 °C, a significant rise in the CR was found. Consistent with NACE RP0775-2005, the corrosion rates are identified as high in the temperatures of 20 and 25°C (5-10 mpy) and severe in the temperatures of above 30 °C for the CR is greater than 10 mpy. The rise of metal dissolution by increasing temperature increases the oxidation-reduction reaction and current density which results in such behavior.

EIS measurements were done to further evaluate the electrochemical corrosion behavior of low-carbon steel in CPS at different temperatures at 4.5 ppm of DO, and to confirm the results achieved through Tafel plots. In this work, the standard EIS system was used in the range of frequencies from 1mHz to 10kHz at the open-circuit voltage with ±10mV perturbation.

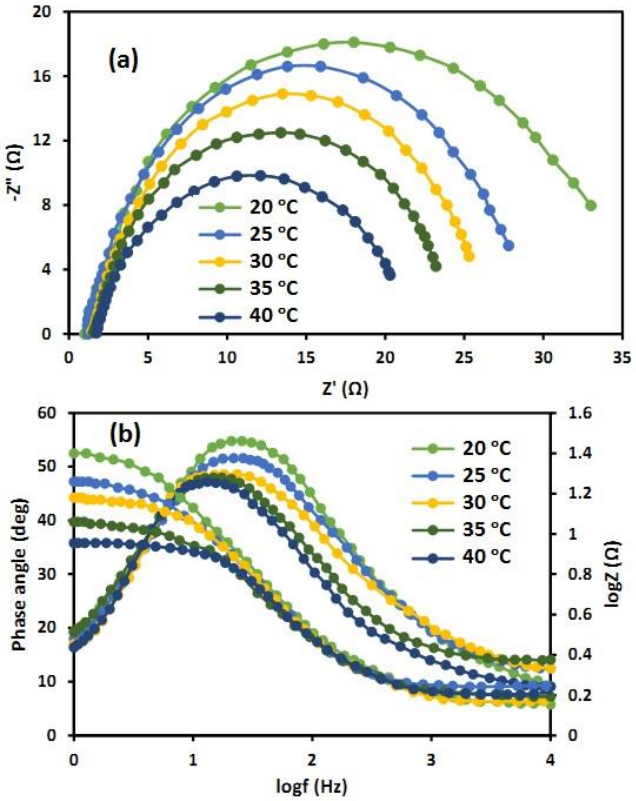

Figure 6. The Nyquist and Bode plots of AISI 1018 low-carbon steel in corrosive environment of concrete pore solution at different temperatures at 4.5 ppm of dissolved oxygen

Figure 6 indicates the Nyquist and Bode plots of AISI 1018 low-carbon steel in the corrosive environment of CPS at different temperatures. The Nyquist plots show a semicircular loop whose diameter rises with reduced temperature, indicating a reduction in corrosion rate of low-carbon steel. Nyquist curves indicate the characteristic shape of semicircles showing that the corrosion procedure is in activation control. The greater diameter of the semicircles achieved by lower temperatures reveals high electrical-resistance at the interface solution-metal, which is due to the oxidation of Fe^{+2} ions and

iron in the CPS. The existence of a capacitive loop typically shows that the surface of steels is partially covered by corrosion products. The EIS plots at all temperatures were revealed to be the same in shape with a diameter of a capacitive loop which reduces with temperature. These results are compatible with those previously research done by other researchers [22].

The Echem Analyst program was used to analyze EIS data at various temperatures using the analogous circuit shown in Figure 3. R_{ct} is the charge-transfer resistance; it is really the resistance of an electron to adjust phases, for example, from either the electrode into solution as well as, more precisely, to a species fixed in the solution. With the purpose of achieving a perfect fit, the double-layer capacitance is correlated with the modification of constant phase elements [23, 24].

Table 4. EIS parameters of low-carbon steel in concrete pore solution in different temperature at 4.5 ppm of dissolved oxygen

Temperature (°C)	$R_s(\Omega)$	$R_f(\Omega)$	C_f (mFcm^{-2})	$R_{ct}(\Omega)$	C_{dl}(mFcm^{-2})
20	12.4	28	14.9	37	19.7
25	8.5	25	18.1	29	23.4
30	7.8	22	21.4	27	25.2
35	9.2	19	23.6	24	28.7
40	8.4	15	26.2	21	31.3

The circuit's fitting values indicate that both R_{ct} and R_s fall with increasing temperature, with the lowest values achieved at the highest temperature (40 °C), indicating an increased corrosion rate with increasing temperature. [25, 26]. The results of the EIS analyses agree with the results gained from the polarization curves. Table 4 summarizes the simulated circuit parameters of low-carbon steel corrosion in CPS.

4. CONCLUSIONS

The effect of environmental conditions such as DO and temperature on electrochemical corrosion behavior of AISI 1018 low-carbon steel in CPS was investigated. The corrosion behavior of low-carbon steel was determined using EIS and potentiodynamic polarization methods at temperatures ranging from 20 to 40 °C and DOES concentration from 0.5 ppm to 4.5 ppm. The corrosion rate of steels increased with increasing ambient temperatures. The electrochemical corrosion resistance was observed to be higher in CPS with lower DO concentrations. The SEM analysis shows that the metal dissolution rate was more intense in CPS with higher DO levels.

References

1. S. Kakooei, H.M. Akil, M. Jamshidi and J. Rouhi, *Construction and Building Materials*, 27 (2012) 73.

2. A. Akbari, M. Nikookar and M. Feizbahr, *Research in Civil and Environmental Engineering*, 1 (2013) 287.
3. Y. Ming, P. Chen, L. Li and C. Hu, *International Journal of Electrochemical Science*, 15 (2020) 9003.
4. S. Kakooei, H.M. Akil, A. Dolati and J. Rouhi, *Construction and Building Materials*, 35 (2012) 564.
5. J. Shi, J. Ming and M. Wu, *Cement and Concrete Composites*, 108 (2020) 103532.
6. M. Feizbahr, S.M. Mirhosseini and A.H. Joshaghani, *Express Nano Letters*, 1 (2020) 1.
7. U.M. Angst, M.R. Geiker, M.C. Alonso, R. Polder, O.B. Isgor, B. Elsener, H. Wong, A. Michel, K. Hornbostel and C. Gehlen, *Materials and Structures*, 52 (2019) 1.
8. R. Hay and C.P. Ostertag, *Cement and Concrete Composites*, 110 (2020) 103573.
9. L. Mengasini, M. Mavroulidou and M.J. Gunn, *Sustainable Chemistry and Pharmacy*, 20 (2021) 100380.
10. V. Chuvil'deev, V. Kopylov, A. Nokhrin, A. Bakhmet'ev, N. Sandler, P. Tryaev, N. Kozlova, N.Y. Tabachkova, A. Mikhailov and M. Chegurov, *Technical Physics Letters*, 43 (2017) 5.
11. M. Feizbahr, J. Jayaprakash, M. Jamshidi and C. Keong, *Middle-East Journal of Scientific Research*, 13 (2013) 1312.
12. W.-C. Baek, T. Kang, H.-J. Sohn and Y.T. Kho, *Electrochimica acta*, 46 (2001) 2321.
13. G.D. Eyu, G. Will, W. Dekkers and J. MacLeod, *Applied Surface Science*, 357 (2015) 506.
14. M. Tachibana, K. Ishida, Y. Wada, R. Shimizu, N. Ota and N. Hara, *Journal of nuclear science and technology*, 49 (2012) 551.
15. D.M. Santos, C.A. Sequeira and J.L. Figueiredo, *Química Nova*, 36 (2013) 1176.
16. Y. Yang, H. Zeng, S. Xin, X. Hou and M. Li, *Corrosion Science*, 165 (2020) 108383.
17. K.-H. Chew, R. Kuwahara and K. Ohno, *Physical Chemistry Chemical Physics*, 20 (2018) 1653.
18. F.F. Eliyan, E.-S. Mahdi and A. Alfantazi, *Corrosion Science*, 58 (2012) 181.
19. H. Sun, B. Shi, F. Yang and D. Wang, *Water Research*, 114 (2017) 69.
20. P. Divya, S. Subhashini, A. Prithiba and R. Rajalakshmi, *Materials Today: Proceedings*, 18 (2019) 1581.
21. E. Machnikova, K.H. Whitmire and N. Hackerman, *Electrochimica acta*, 53 (2008) 6024.
22. X. Wang, J. Xu, C. Sun and M. Yan, *International Journal of Electrochemical Science*, 10 (2015) 8656.
23. Y. Maocheng, X. Jin, Y. Libao, W. Tangqing, S. Cheng and K. Wei, *Corrosion Science*, 110 (2016) 23.
24. M. Tan, F. Varela, Y. Huo, F. Mahdavi, M. Forsyth and B. Hinton, *Corrosion and materials*, 42 (2017) 70.
25. A. Benamor, A.G. Talkhan, M. Nasser, I. Hussein and P.C. Okonkwo, *Journal of Electroanalytical Chemistry*, 808 (2018) 218.
26. M. Desimone, G. Gordillo and S.N. Simison, *Corrosion Science*, 53 (2011) 4033.